Rapid Study on Healthcare Applications

S. Sowmyayani,
Assistant Professor,
Department of Computer Science (SF),
St. Mary's College (Autonomous), Thoothukudi, Tamilnadu.
sowmyayani@gmail.com

Abstract

The advancement of computer-aided design helps the medical force and security force. Some applications include biometric recognition, elderly fall detection, face recognition, cancer recognition, tumor recognition, etc. This paper deals with different machine learning algorithms that are more generically used for any health care system. The most focused problems are classification and regression. With the rise of big data, machine learning has become particularly important for solving problems. Machine learning uses two types of techniques: supervised learning, which trains a model on known input and output data so that it can predict future outputs; and unsupervised learning, which finds hidden patterns or intrinsic structures in input data. Clustering is the most common unsupervised learning technique. Classification and regression are supervised learning techniques. The above-mentioned models are discussed briefly, and the pre-trained network models are explained in this chapter.

Keywords: Supervised Learning, Unsupervised Learning, Regression, Neural Network

I. INTRODUCTION TO HEALTHCARE APPLICATIONS

The recent advancements in computing, machine learning, and image recognition have a significant impact on the automatic detection of various diseases. Several screening approaches are now used to detect suspicious diseases. Computer-aided diagnosis (CAD) is able to assist doctors in understanding medical images, allowing for cancer diagnosis with greater accuracy, which is critical for patients. Deep Convolutional Neural Networks (DCNN) has been proven to perform well in image classification, object detection, and other visual tasks. They have found great success in medical imaging applications.

Computational techniques have a great impact in the fields of medicine and biology. These techniques help medical practitioners diagnose any abnormality in advance and

provide fruitful treatment. There are various diseases that can be cured when treated early. This chapter discusses various health care applications that can be solved using CAD. The architecture of all those applications follows the same procedure.

1.1 Conventional Architecture

The traditional architecture of any classification system follows the same procedure. Supervised learning trains the dataset before testing. Hence, the dataset is divided into training and testing sets. In both training and testing, there are four important phases. They are preprocessing, segmentation, feature extraction, and classification. This section briefly discusses all these phases. Machine learning feature extraction and classification are elaborated in [1]. Figure 1 shows the conventional architecture of classification model.

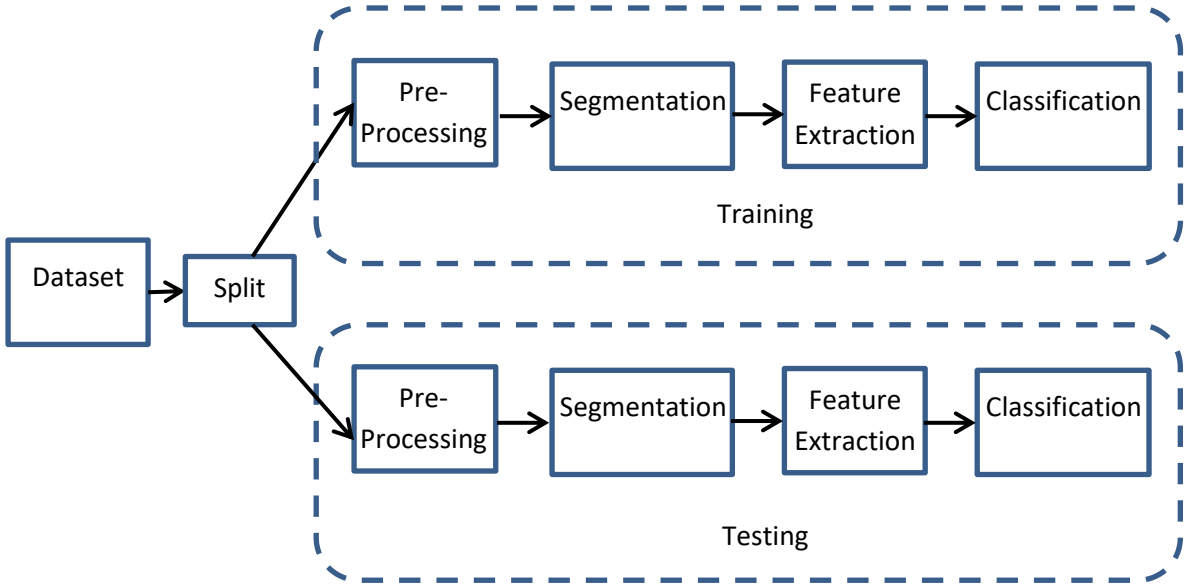

Fig. 1 Conventional Architecture of Classification Model

Data Splitting

The dataset is split into training and testing tests. The splitting is done in a random ratio. Most of the classification systems follow 80:20 ratio for training and testing. Other ratios are 90:10, 70:30, 60:40, and 50:50. The greater the training dataset, the more accurate the classification will be. But a good classification system should give accurate results even with less training.

Pre-Processing

Initially, preprocessing is done to improve the quality of image visualization. After capturing the digital image and prior to instigating algorithm applications, each image should be assessed with regard to its common elements like noise, background, brightness, blur, intensity variations etc. This work is effectively done through a preprocessing step. This step improves the performance of the classification system.

Segmentation

Image segmentation is the process of dividing the images into objects or groups. In medical images, the affected area should be segmented to identify whether the disease is severely affected. Detecting cancerous cells as quickly as possible can potentially save millions of lives. Image segmentation techniques can be broadly classified as region-based segmentation, edge-based segmentation, clustering-based segmentation, and mask R-CNN.

Region based Segmentation

In region-based segmentation, the objects are segmented into different regions based on some threshold value(s). There may be a global threshold and a local threshold. When the object and background have high contrast, this method performs really well. This method is very simple and fast. The major drawback is that when there is no significant grayscale difference or an overlap of the grayscale pixel values, it becomes very difficult to get accurate segments.

Edge based Segmentation

This method makes use of discontinuous local features of an image to detect edges and hence define the boundary of the object. It is good for images to have better contrast between objects. Edge-based segmentation is not suitable when there are too many edges in the image or if there is less contrast between objects.

Clustering based Segmentation

This method divides the pixels of the image into homogeneous clusters. It works really well on small datasets and generates excellent clusters. The major drawback is that the computation time is too large and expensive. K-means is one algorithm which is not suitable for clustering non-convex clusters.

Mask R-CNN

This method gives three outputs for each object in the image: its class, bounding box coordinates, and object mask. It is simple and flexible. It is also the current state-of-the-art for image segmentation. This method suffers from high training time.

Feature Extraction

Feature extraction refers to the process of transforming raw data into numerical features that can be processed while preserving the information in the original data set. It yields better results than applying machine learning directly to the raw data.

Feature extraction can be accomplished manually or automatically:

- Manual feature extraction requires identifying and describing the features that are relevant to a given problem and implementing a way to extract those features. In many situations, having a good understanding of the background or domain can help make informed decisions as to which features could be useful. Over decades of research, engineers and scientists have developed feature extraction methods for images, signals, and text.
- Automated feature extraction uses specialized algorithms or deep networks to automatically extract features from signals or images without the need for human intervention. This technique can be very useful when you want to move quickly from raw data to developing machine learning algorithms.

With the ascent of deep learning, feature extraction has been largely replaced by the first layers of deep networks – but mostly for image data. For signal and time-series applications, feature extraction remains the first challenge that requires significant expertise before one can build effective predictive models.

The feature extraction algorithm produces a vector that contains a list of features. This is called a "feature vector," which is a 1D array that makes a robust representation of the object. It is important to point out that the 1D array represents just one car. A very important characteristic of a feature is repeatability. Actually, the feature should be able to detect objects in general, not just this specific one. So, in real world problems, the feature will not be an exact copy of the piece in the input image.

The feature will not look exactly like the feature of just one object. Instead, it looks like it has features similar to all the features in the training dataset. When the feature extractor sees thousands of similar objects, it recognizes patterns that define the object in general, regardless of where they appear in the image and what type of object it is.

Classification

Image classification is a complex procedure which relies on different components. Here, some of the presented strategies, issues, and additional prospects of image orders are addressed. The primary spotlight will be on cutting-edge classification methods, which are utilized for enhancing characterization precision. There are several classifier models introduced so far.

2. Health Care Applications

Here are some important health care applications that can be diagnosed if it is treated earlier. Machine helps to identify the disease earlier than the human.

2.1 Brain Tumor Detection

Brain tumor segmentation is the main procedure for early tumor diagnosis and radiotherapy scheduling. Though several brain tumor segmentation methods have been available, proficient tumor segmentation methods are still challenging because brain tumor images exhibit complex characteristics. In addition to tumor heterogeneity, tumor edges can be complex and visually vague. Brain tumor analysis is done by doctors, but its grading gives different conclusions, which may vary according to the expertise of the doctor.

Brain tumors are a heterogeneous group of central nervous system neoplasms that arise within or adjacent to the brain. Moreover, the location of the tumor within the brain has a profound effect on the patient's symptoms, surgical therapeutic options, and the likelihood of obtaining a definitive diagnosis. The location of the tumor in the brain also markedly alters the risk of neurological toxicities that alter the patient's quality of life. At present, brain tumors are detected by imaging only after the onset of neurological symptoms. No early detection strategies are in use, even in individuals known to be at risk for specific types of brain tumors by virtue of their genetic makeup.

Current histopathological classification systems, which are based on the tumors' presumed cell of origin, have been in place for nearly a century and were updated by the

World Health Organization (WHO) in 1999. Although satisfactory in many respects, they do not allow accurate prediction of tumor behavior in the individual patient, nor do they guide therapeutic decision-making as precisely as patients and physicians would hope and need. Current imaging techniques provide meticulous anatomical delineation and are the principal tools for establishing that neurological symptoms are the consequence of a brain tumor.

Magnetic Resonance Imaging (MRI) is a medical technique mainly used by radiologists for the visualization of internal structures of the human body without any surgery. MRI provides ample information about the human soft tissue, which helps in the diagnosis of brain tumors. Accurate segmentation of MRI images is important for the diagnosis of brain tumors by computer-aided clinical tools. After appropriate segmentation of brain MR images, tumors are classified as malignant or benign, which is a difficult task due to complexity and variation in tumor tissue characteristics like shape, size, gray level intensities, and location.

2.2 Diabetic Retinopathy

The primary effect of Diabetic Retinopathy (DR) is that it can cause vascular damage to the retina before the patient develops more severe symptoms. The damage on the retina is not uniformly distributed, which means the relation of pupil response to light stimulus on the center of the retina and on the peripheral of the retina will be different for a patient with DR than for a healthy person. Images of the ocular fundus, i.e., retinal images, can assist in the diagnosis and treatment of retinal, ophthalmic, and even systemic diseases, such as diabetes, hypertension, and arteriosclerosis. Automatic detection of lesions in retinal images can assist in early diagnosis and screening of diabetic retinopathy. Exudates are the primary sign of DR. So, detection of exudates is the fundamental requirement to diagnose the progress of DR.

Premature detection of DR is a challenging task because patients with DR will have no symptoms until vision loss develops. DR is a progressive disease; it becomes Proliferative Diabetic Retinopathy (PDR) from Non-Proliferative Diabetic Retinopathy (NPDR). NPDR is the earliest stage of DR, while PDR is the most advanced stage. This can be identified in the screening process, which is done yearly for diabetic patients looking for any signs of NPDR. It has been shown that fundus photography is the most accurate means of screening for retinopathy. In most developing countries, the rural areas will not have enough specialists to examine diabetic patients by ophthalmologists in screening programs.

NPDR, commonly known as background retinopathy, is an early detection of DR. The DR starts with a mild NPDR, which usually does not affect the vision. When lipoproteins or other proteins leak from retinal blood vessels, it affects the vision, which is called exudates (EXs). Exudates can be hard exudates (yellow spots seen in the retina) or soft exudates (pale yellow or white areas with ill-defined edges).

2.3 Glaucoma Detection

Glaucoma is an eye disease that occurs due to the intraocular pressure inside the eye triggered by the secretion of excess fluid, which in turn leads to damage of the optic nerve. This can impair vision by causing irreversible damage to the optic nerve and to the retina. This will lead to blindness if it is not detected at an earlier stage. Glaucoma results in vision loss and is an especially dangerous eye condition because it frequently progresses without noticeable symptoms. Early glaucoma is complicated to detect, requiring a suspicious examination of the optic nerve. The detection of glaucoma through Optical Coherence Tomography (OCT) and Heidelberg Retinal Tomography (HRT) is very costly [2, 3], compared to digital fundus images. It is easy to extract the features of the fundus images such as the optic disc and cup to suspect glaucoma [4, 5, 6].

Glaucoma detection is classified into two categories: primary open angle glaucoma and secondary glaucoma. At a very early stage, if it is diagnosed as glaucoma, that stage is called primary open angle glaucoma. If it is diagnosed at a later stage, it is secondary glaucoma. Glaucoma detection is generally done using an Optic Nerve Head (ONH) that uses stereo optic disc images for structural abnormalities. The stereo optic disk images are obtained by stereo photographs, which give the perception of the cup depth. This depth is a very important indication for glaucoma.

There is much research in monocular stereo optic images. These images are used to determine the changes in the optic nerve by computing the ONH depth map with stereo matching methods [7-8]. Cup-to-Disc Ratio (CDR) is the commonly-used parameter which is calculated from the optic disc and cup and is commonly used to identify the elongation of the optic cup and loss of neuro-retinal rim.

2.4 Mammogram Abnormalities

Breast cancer is one of the most prevalent cancers among women [9], and it shows high mortality rates too. Human lives can be saved when the cancer is detected at an early

stage. Mammography is a boon to medical science because it captures an image of the breast tissue. With this aid, the physician can detect breast cancer earlier. Thus, a mammogram acts as a screening tool for breast cancer detection. The earliest symptom of breast cancer is the group of calcifications.

Generally, microcalcification is a tiny deposit of calcium that is present in the breast tissue. This calcium deposit can be of a circular, lobular, specular, or irregular shape. These microcalcifications can be observed in a mammogram as small granules and it is very difficult for the physician to locate them accurately. According to one study, doctors ignore ten to forty percent of microcalcifications [10-11]. However, computers can detect the abnormalities easily, provided the system is trained effectively. By implementing advanced image processing techniques, an effective CAD system can help physicians detect cancer earlier [12]. In [13], three different features are extracted from the segmented mammogram image, which is classified using an Extreme Learning Machine (ELM) classifier.

Several CAD systems have already been reported in the literature. Most of the existing systems suffer from high false positive and negative rates. Thus, there is a constant need and demand for a CAD system to detect breast cancer.

2.5 Fall Detection

The occurrence and detection of falls are increasing in elderly people. This requires researchers and healthcare professionals to create an efficient method in order to detect and prevent these uncertain situations. The WHO stated that the effects of falls are growing worldwide. From their report, it is clear that around 28–35% of people of age 65 fall every year, and within that, 32-42% of people are of age 70. The fall rate increases as the number of elderly people increases. Approximately, in the year 2050, more than one in each group of five individuals will likely be aged 65 years or above. This will probably stimulate an increased fall rate. Hence, it is necessary to develop fall detection systems to avoid these incidents. An efficient fall detection method is designed with correlation and motion history images [14], which is followed by a keyframe based fall detection for elderly care systems in 2021 [15].

The causes of falls are due to factors related to behavior, factors related to the person and factors related to the environment. There is a need for assistance to avoid these factors arising.

2.6 Lung Cancer Detection

As reported by WHO, cancer has caused a very large number of deaths, approximately 8.8 million deaths in 2015. Almost 20% or 1.69 million deaths are due to lung cancer. Cancer screening plays an important role in preventive care because cancer is most treatable when caught in the early stages. The appearances of the malignant lung nodules more commonly demonstrate a spiculated contour, lobulation, and inhomogeneous attenuation. Presently, Low Dose Computed Tomography (LDCT) plays an important role in screening lung cancer.

LDCT screening has reduced lung cancer deaths and is recommended for highrisk demographics. Results from LDCT screening may be further evaluated with standard dose Computed Tomography (CT). However, there are many barriers to implementing LDCT screening, such as providers' anxiety on the access to LDCT equipment and potential financial burdens in rural populations. Moreover, rural populations have limited access to both primary care physicians and specialists. On the other hand, chest x-rays are readily available in rural areas. Nonetheless, chest x-rays produce lower quality images compared to LDCT or CT scans and, therefore, a lower quality diagnosis is generally expected.

2.7 Skin Cancer Detection

Cancer [16–18] is one of the most difficult challenges of modern medicine. It begins when cells in a part of the body grow extraordinarily and out of control. These cancer cells take up the nutrients from the normal strong cells. Hence, the strong cells die off, the body gets weaker and the immune system is no longer able to protect the body. These cancer cells can metastasize from this part to other parts of the body. There are several parts of the body that may be affected by cancer, such as the liver, lung, bone, breast, prostate, bladder, and rectum, and the skin can also be affected by cancer.

Skin cancer can be classified into two groups: melanoma and non-melanoma [19-20]. According to WHO statistics, there were between two and three million non-melanoma skin cancers and 132,000 melanoma skin cancers worldwide in 2017. Melanoma skin cancer is the fastest growing form of skin cancer, and it causes the most deaths among forms of skin cancer. Basically, all forms of skin cancer can be cured by radiation therapy, chemotherapy, immunotherapy, etc., or their combination, but the treatment regimen will be more effective if patients are diagnosed and treated early.

For melanoma skin cancer, the ABCD rule (Asymmetry, Border, Colour, Diameter) [21] is used for detecting melanoma. Skin lesion segmentation methods include color channel optimization [22-24], level set-based methods [25-26], iterative stochastic regions merging [27], deep learning with convolution neural networks [28-33], and others. On one hand, the accuracy of segmentation methods based on various color channels optimization and based on level set methods is usually not high. Further, the final results are affected by different factors such as hairs and marked signs by pens/rules, and these methods fail to reliably segment very low-density regions, etc. On the other hand, recent deep learning-based methods require a large amount of training data and extensive computational time and resources. Moreover, to obtain good accuracy in supervised deep learning models, large-scale training data incorporating the various factors mentioned above is paramount in obtaining final segmentations.

3. RESULTS DISCUSSION

3.1 Segmentation Results

This section discussion the graphical results obtained in health care applications discussed in the previous section. Figure 2 shows the optic disc and cup segmentation of glaucoma detection results.

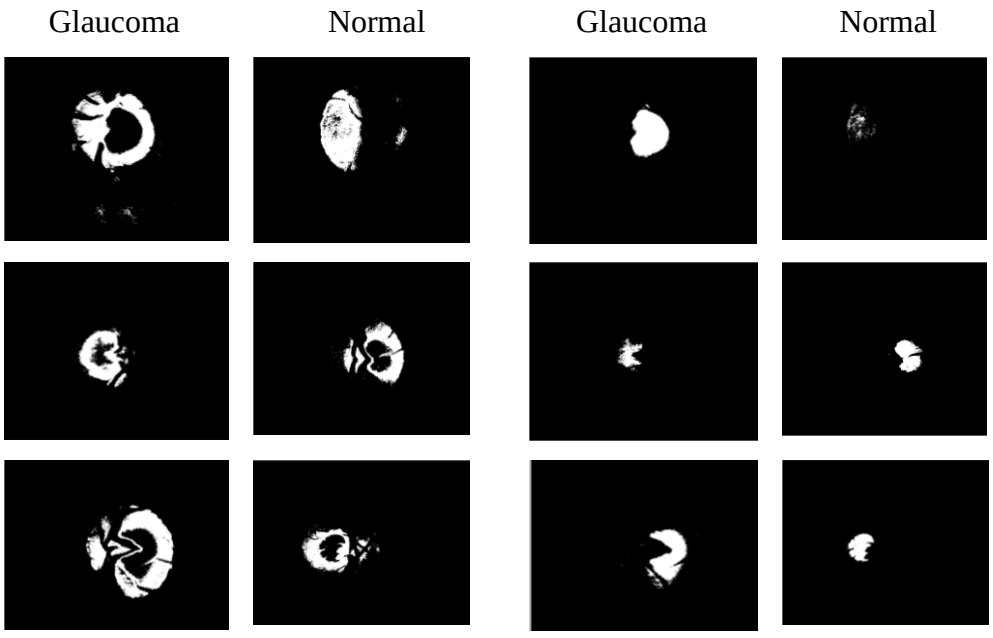

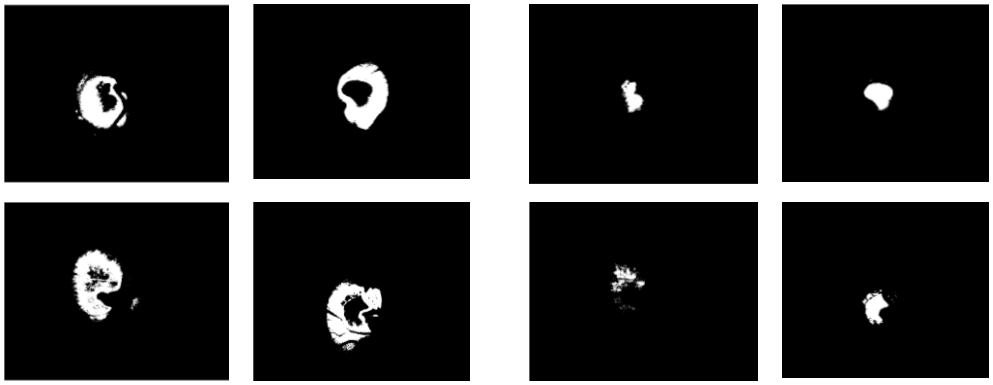

Fig. 2 Left 2 columns optic disc segmentation and Right 2 columns optic cup segmentation

It is observed that the size of the cup of glaucoma suspect eyes is larger than the normal eyes. Figure 3 shows the affected regions in mammogram images. The malignant and benign tumor regions are segmented in Fig. 4.

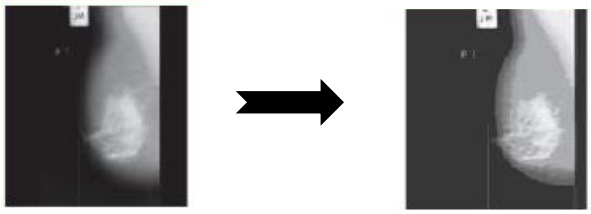

(a)

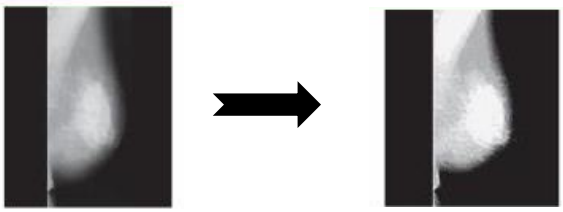

(b)

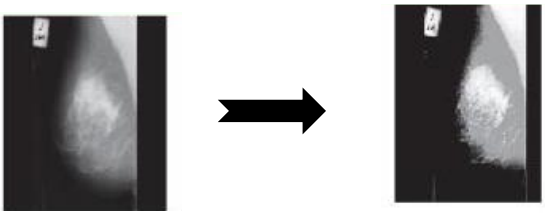

(c)

Fig. 3 Input and its Segmented Image (a) Normal (b) Benign (c) Malignant Mammograms

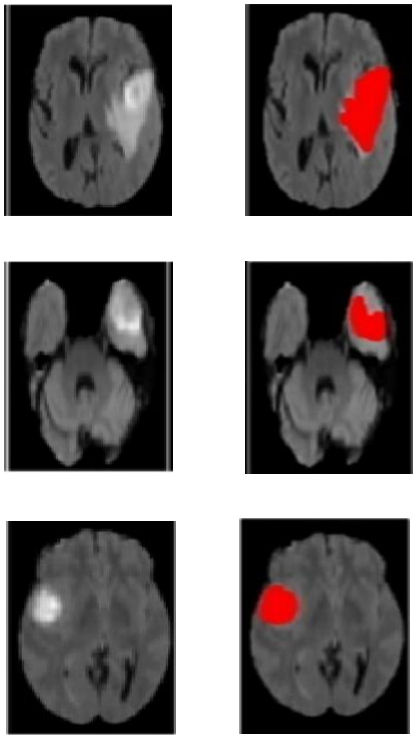

Fig. 4 Tumor Segmentation in MRI Images (Left column indicates Original Image and the Right Column indicates Segmented Image)

Figure 5 shows the hard exudates detection in eye images. Lungs and its segmented images are shown in Fig. 6. The skin cancer segmentation results are shown in Fig. 7.

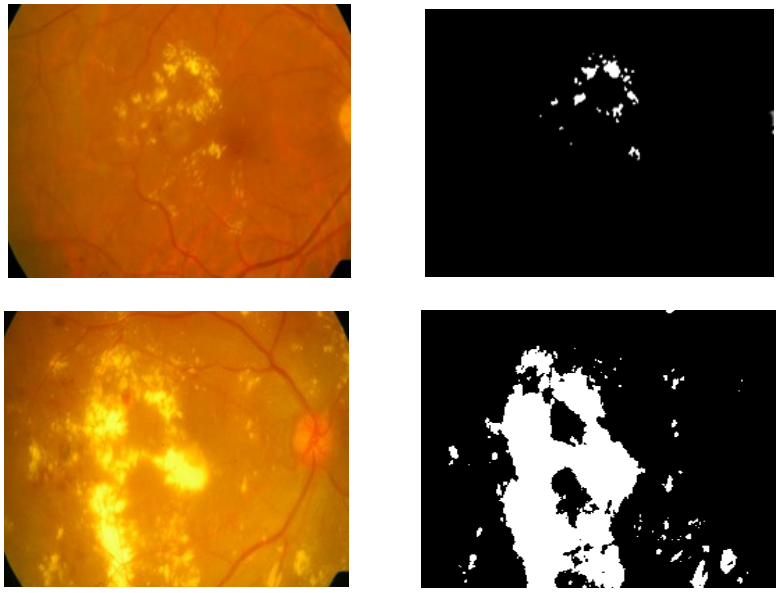

Fig. 5 Fundus images and the detection of hard exudates results

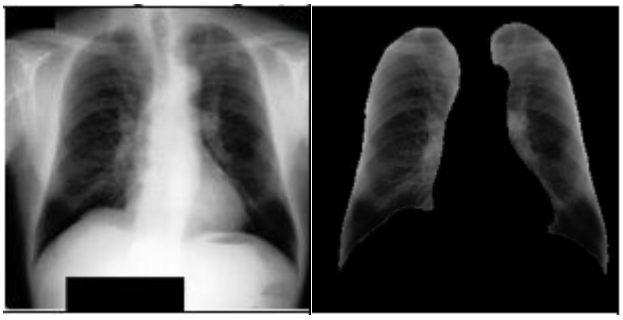

Fig. 6 Original Lung and its Segmented Image

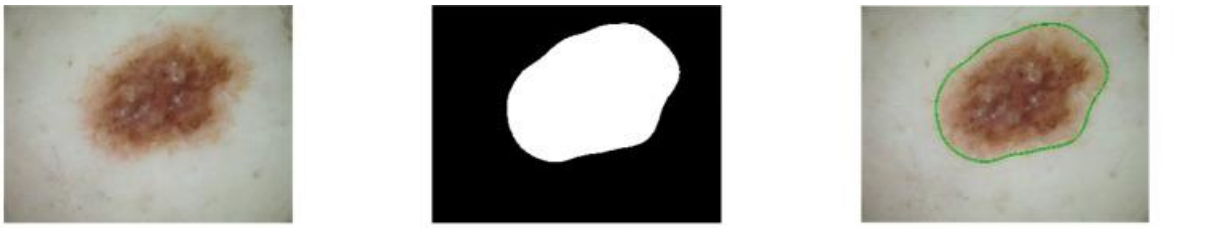

a) Input image in RGB

b) Binary-segmented region by the normalized red band

c) Segmented boundary by the normalized red band

Fig. 7 Skin Cancer Segmentation Results

3.2 PERFORMANCE MEASURES

The classification models are evaluated using some important performance metrics such as accuracy, precision, recall, etc. which are discussed in this section. These metrics use confusion matrix as its base.

6.2 Confusion Matrix

It is used for finding the correctness and accuracy of the model. It is also used for Classification problem where the output can be of two or more types of classes. Figure 8 shows the confusion matrix with all the values.

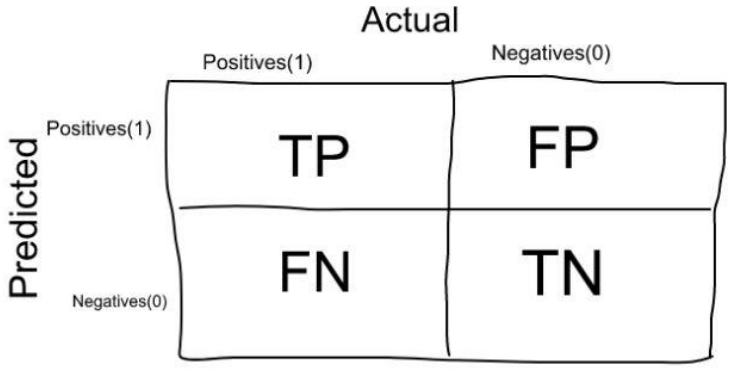

Fig. 8 Confusion Matrix

True Positives (TP): The cases when the actual class of the data point was 1(True) and the predicted is also 1(True).

True Negatives (TN): The cases when the actual class of the data point was 0(False) and the predicted is also 0.

False Positives (FP): The cases when the actual class of the data point was 0(False) and the predicted is 1(True).

False Negatives (FN): The cases when the actual class of the data point was 1(True) and the predicted is 0(False).

6.3 Metrics

To analyze the performance of the segmentation methods, accuracy, Positive Predictive Value (PPV), Dice Similarity Coefficient (DSC), Jaccard Index (JI), Sensitivity and Specificity are used.

Accuracy is defined as the closeness of agreement between a measured quantity value and a true quantity value of a measurand (i.e., the quantity intended to be measured) (ISO-JCGM 200, 2008), and is often limited by calibration errors. To find the percentage of the overlapped region of the ground-truth and segmented region, precision rate is used. The **PPV** is the portion of extracted illustrations that are related to locate. The **Sensitivity** is the portion of related illustrations that are extracted in relation to the uncertainty.

F-measure rate is the division of multiplicative values of precision and recall to the addition of precision and recall. **Specificity** measures the proportion of negatives which are correctly identified. **DSC** finds matches between the segmented region and ground-truth image. It finds how much similarity existed when the segmented region is overlapped with the ground-truth image. The **JI** is calculated as the amount of the intersection of the affected and non-affected pixels divided by the amount of their combination. Table 1 displays the formula for all the above-mentioned metrics.

Table 1 Formula for the Metrics

Measure	Formula

Accuracy	$Ac_r = \frac{TP + TN}{TP + TN + FP + FN} \times 100$
PPV	$PPV = \frac{TP}{TP + FP}$
Sensitivity	$Sensitivity = \frac{TP}{TP + FN}$
Specificity	$\text{Specificity} = \frac{\text{TN}}{(\text{FP} + \text{TN})}$
DSC	$DSC = \frac{2 \times TP}{FP + (2 \times TP) + FN}$
JI	$JI = \frac{TP}{TP + FP + FN}$

3.3 COMMON DATASETS

This section discusses some of the common datasets used in each healthcare application. Most of the mentioned datasets are publicly available. Table 2 summarizes the common dataset of the discussed healthcare applications.

Table 2 Common Datasets

Application	Common Datasets
Brain Tumor Detection	BRATS 2012, 2013, 2014, 2015, 2016, 2017, 2018, 2019, 2020 [34]
Glaucoma Detection	RIM-ONE [35], ACRIMA [36], ORIGA [37], HRF [38], Drishti-GS1 [39], sjchoi86-HRF [40]
Diabetic Retinopathy	IDRiD [41], DRIVE [42], Messidor-2 [43]
Mammogram Abnormalities	MIAS [44], DDSM [45]
Fall Detection	Video-based Datasets: UP Fall [46], MobiFall [47],
Lung Cancer	JSRT [48], ChestX-ray14 [49, 50]
Skin Cancer	ISIC [51]

Table 3 displays the common datasets used in brain tumor segmentation. Table 4 and 5 gives the common datasets and recent results obtained in Glaucoma detection and diabetic retinopathy methods respectively.

Table 3 Common Datasets in Brain Tumor Detection

Dataset	Description	Accuracy (%)
BRATS 2012	3875 training, 3875 testing	100 [52]
BRATS 2013	4650 training, 1550 testing	92.2 [52]
BRATS 2014	3000 training, 15500 testing	98.5 [52]
BRATS 2015	Size 240 x 240 x 155 32,020 training and 24,180 testing	99.09 [53]
BRATS 2016	19032 non-glioma 15272 glioma	99.45 [53]
BRATS 2017	210 images	99.54 [53]
BRATS 2018	29605 training, 10320 testing	92.67 [54]

Table 4 Common Datasets in Glaucoma Detection

Dataset	Description	Results
RIM-ONE	Size 2144x 1424 85 are normal eyes, and 74 are glaucomatous eyes	96.1% DSC for disc and 84.45% DSC for cup [55]
ACRIMA	396 glaucoma and 309 non-glaucoma	0.77 AUC [56]
ORIGA	Size between 1944×2108 and 2426×3007 pixels. 296 glaucoma and 724 non-glaucoma	0.85 AUC [57]
HRF	27 glaucoma and 18 non-glaucoma	0.95 AUC [56]
Drishti-GS1	2896 x 1944 70 glaucoma and 31 non-glaucoma	97.38% DSC for Disc and 88.77% DSC for cup [55]
sjchoi86-HRF	101 glaucoma and 300 non-glaucoma	0.85 AUC [56]

Table 5 Common Datasets in Diabetic Retinopathy

Dataset	Description	Results
IDRiD	516 images	0.95 AUC [58]
DRIVE	33 normal and 7 abnormal	97.5% Accuracy [59]
Messidor-2	1748 images	0.95 AUC [58]

In Table 4 and 5, AUC denotes Area Under ROC Curve. ROC is a Receiver Operating Characteristics which is plot between true positive rate and false positive rate. Table 6 and 7 shows the datasets and the results obtained by mammogram abnormalities detection and fall detection methods respectively.

Table 6 Common Datasets in Mammogram Abnormalities

Dataset	**Description**	**Results**
MIAS	322 images of size 1024 x 1024, 204 normal 118 abnormal	Accuracy 98.2% [60]
DDSM	5282 training, 278 testing	0.85 AUC [61]

Table 7 Common Datasets in Fall Detection

Dataset	**Description**	**Accuracy (%)**
UP Fall	17 subjects	95.1 [62]
MobiFall	24 subjects	99.12 [62]

In the above tables, the accuracy is higher than 95%. It shows the performance of the good classification models. Table 8 and 9 shows the common datasets and the results obtained by lung cancer and skin cancer detection methods respectively.

Table 8 Common Datasets in Lung Cancer

Dataset	**Description**	**Results**
JSRT	247 images 154 abnormal, 93 normal	97.5 DSC [63]
ChestX-ray14	112120 images	0.94AUC [64]

Table 9 Common Datasets in Skin Cancer

Dataset	**Description**	**Results**

ISIC	23000 images	95% AUC [65]

4. CONCLUSION

Researches are developing in the field of medicine over past few decades. This paper discusses some common health care applications. It also elaborates each phases in segmentation and classification models. An overview is given to the common datasets and the performance metrics used to evaluate the classification models. This paper helps the junior researches in developing the best classification model for health care applications. It also guides to get the datasets for various applications.

References:

[1] Sowmyayani. S, 2022, Machine Learning. In Kumar, A., Sagar, S., Kumar, T.G. and Kumar, K.S. eds., 2022. *Prediction and Analysis for Knowledge Representation and Machine Learning*. CRC Press.

[2] Acharya, U. R., Ng, E.Y.K., and Suri, J. S., "Image modeling of human Eye" Artech House, 2008.

[3] U.R., Chau, K. C., Ng, E. Y. K., Wei, W., and Chee, C., "Application of higher order spectra for the identification of diabetes retinopathy stages". J. Medsyst.

[4] Song, X., Chen, Y., Song, K., and Chen, Y., "A Computer – based diagnosis of glaucoma using an artificial neural network". Proceedings of 17th Annual Conference IEEE Engineering in Medicine and Biology, 1, 847-848, 1995..

[5] Viranee Thongnuch, Bunyarit Uyyanonvara, "Automatic optic disc detection from low contrast retinal images of ROP infant using mathematical morphology", 2000.

[6] Nayak, J. Bhat, P.S., Acharya, U. R., Lim, C.M., and Kagathi, M., "Automated identification of different stages of diabetic retinopathy using digital fundus images". J. Med. Sys., 2008.

[7] L. Tang, et al., "Robust Multiscale Stereo Matching from Fundus Images with Radiometric Differences," IEEE Transactions on Pattern Analysis and Machine Intelligence, vol. 33, no. 11, pp. 2245–2258, Nov. 2011.

[8] T. Nakagawa, et al., "Quantitative depth analysis of optic nerve head using stereo retinal fundus image pair," J. Biomed. Opt, vol. 13, no. 6, pp. 064026–064026–10, 2008.

[9] URL: http://www.who.int/whosis/mort/en/index.html, 2006.

[10] R.G.Bird, T.W.Wallace, B.C.Yankaskas, "Analysis of cancers missed at screening mammography," Radiology, vol. 184, pp. 613–617,1992

[11] H. Burhenne, L. Burhenne, F. Goldberg, T. Hislop, A.J.Worth, P.M.Rebbeck, and L.Kan, "Interval breast cancers in the screening mammography program of British Columbia: Analysis and classification," Am. J Roentgenol., vol. 162, pp.1067–1071,1994

[12] Lee SK, Lo CS, Wang CM, Chung PC, Chang CI, Yang CW, Hsu PC: A computer-aided design mammography screening system for detection and classification of microcalcifications. Int J Med Inform 60(1):29–57, 2000

[13] Sowmyayani, S. and Murugan, V., 2021. Multi-Type Classification Comparison of Mammogram Abnormalities. *International Journal of Image and Graphics*, *21*(03), p.2150027.

[14] Sowmyayani, S., Murugan, V. and Kavitha, J., 2021. Fall detection in elderly care system based on group of pictures. *Vietnam Journal of Computer Science*, *8*(02), pp.199-214.

[15] Sowmyayani, S. and Rani, P.A.J., 2019. An efficient fall detection method for elderly care system. *International Journal of Computer and Information Engineering*, *13*(3), pp.173-177.

[16] "Melanoma: Statistics," American Cancer Society, Jul. 2016. [Online]. Available: https://www.cancer.net/cancer-types/melanoma/statistics. Accessed 6 Nov. 2018

[17] "Melanoma skin cancer," European Commission, 2017. [Online]. Available: https://ec.europa.eu/research/health/pdf/factsheets/melanoma_skin_cancer.pdf. Accessed 6 Nov. 2018

[18] Seyed HH, Mohammadamin D. Review of cancer from perspective of molecular. *Journal of Cancer Research and Practice.* 2017;4(4):127–129. doi: 10.1016/j.jcrpr.2017.07.001.

[19] Yu Lequan, Chen Hao, Dou Qi, Qin Jing, Heng Pheng-Ann. Automated Melanoma Recognition in Dermoscopy Images via Very Deep Residual Networks. *IEEE Transactions on Medical Imaging.* 2017; 36(4): 994–1004. doi: 10.1109/TMI.2016.2642839.

[20] Esteva A, Kuprel B, Novoa RA, Ko J, Swetter SM, Blau HM, Thrun S. Dermatologist-level classification of skin cancer with deep neural networks. *Nature.* 2017; 542:115–118. doi: 10.1038/nature21056.

[21] M. Kunz and W. Stolz, “ABCD rule,” Dermoscopedia Organization, 17 Jan. 2018. [Online]. Available:https://dermoscopedia.org/ABCD_rule. Accessed 11 Nov. 2018

[22] A. A. A. Al-abayechi, X. Guo, W. H. Tan and H. A. Jalab, “Automatic skin lesion segmentation with optimal colour channel from dermoscopic images,” *ScienceAsia,* vol. 40S, pp. 1–7, 2014.

[23] D. N. H. Thanh, U. Erkan, V. B. S. Prasath, V. Kumar and N. N. Hien, “A Skin Lesion Segmentation Method for Dermoscopic Images Based on Adaptive Thresholding with Normalization of Color Models,” in *IEEE* 2019 *6th International Conference on Electrical and Electronics Engineering,* Istanbul, 2019.

[24] D. N. H. Thanh, N. N. Hien, V. B. S. Prasath, U. Erkan, K. Adytia: Adaptive Thresholding Skin Lesion Segmentation with Gabor Filters and Principal Component Analysis,” in *The 4th International Conference on Research in Intelligent and Computing in Engineering RICE'19,* Hanoi, 2019

[25] D. N. H. Thanh, N. N. Hien, V. B. S. Prasath, L. T. Thanh and N. H. Hai, “Automatic Initial Boundary Generation Methods Based on Edge Detectors for the Level Set Function of the Chan-Vese Segmentation Model and Applications in Biomedical Image Processing,” in *The 7th International Conference on Frontiers of Intelligent Computing: Theory and Application (FICTA*-2018*),* Danang, 2018.

[26] Z. Ma and J. M. R. S. Tavares, “Segmentation of Skin Lesions Using Level Set Method,” in *Computational Modeling of Objects Presented in Images. Fundamentals, Methods, and Applications (Lecture Notes in Computer Science, vol 8641)*, Springer, 2014, pp. 228–233.

[27] Wong A., Scharcanski J., Fieguth P. Automatic Skin Lesion Segmentation via Iterative Stochastic Region Merging. *IEEE Transactions on Information Technology in Biomedicine.* 2011;15(6):929–936. doi: 10.1109/TITB.2011.2157829.

[28] Al-Masni MA, Al-Antari MA, Choi MT, Han SM, Kim TS. Skin lesion segmentation in dermoscopy images via deep full resolution convolutional networks. *Computer Methods and Programs in Biomedicine.* 2018;162:221–231. doi: 10.1016/j.cmpb.2018.05.027.

[29] M. Berseth, “ISIC 2017-Skin Lesion Analysis Towards Melanoma,” *arXiv:1703.00523,* 2017.

[30] Y. Yuan, “Automatic skin lesion segmentation with fully convolutional-deconvolutional networks,” *arXiv:1703.05165,* 2017.

[31] L. Bi, J. Kim, E. Ahn, D. Feng and M. Fulham, “Semi-automatic skin lesion segmentation via fully convolutional networks,” in 2017 *IEEE 14th International Symposium on Biomedical Imaging (ISBI 2017)*, Melbourne, 2017.

[32] Jaisakthi SM, Mirunalini P, Aravindan C. Automated skin lesion segmentation of dermoscopic images using GrabCut and k-means algorithms. *IET Computer Vision.* 2018;12(8):1088–1095. doi: 10.1049/iet-cvi.2018.5289.

[33] Burdick J, Marques O, Weinthal J, Furht B. Rethinking Skin Lesion Segmentation in a Convolutional Classifier. *Journal of Digital Imaging.* 2018;31(4):435–440. doi: 10.1007/s10278-017-0026-y.

[34] H. Menze, A. Jakab, S. Bauer, J. Kalpathy-Cramer, K. Farahani, J. Kirby, et al. "The Multimodal Brain Tumor Image Segmentation Benchmark (BRATS)", IEEE Transactions on Medical Imaging 34(10), 1993-2024 (2015) DOI: 10.1109/TMI.2014.2377694

[35] F. Fumero et al., “RIM-ONE: An open retinal image database for optic nerve evaluation,” in Intl. Symposium on Computer-Based Medical Systems (CBMS), 2011.

[36] A. Diaz-Pinto, S. Morales, V. Naranjo, T. Köhler, J. M. Mossi, and A. Navea, “Cnns for automatic glaucoma assessment using fundus images: an extensive validation,” Biomedical engineering online, vol. 18, no. 1, p. 29, 2019.

[37] Z. Zhang, F. S. Yin, J. Liu, W. K. Wong, N. M. Tan, B. H. Lee, J. Cheng, and T. Y. Wong, “Origa-light: An online retinal fundus image database for glaucoma analysis and research,” in 2010 Annual International Conference of the IEEE Engineering in Medicine and Biology. IEEE, 2010, pp. 3065–3068.

[38] A. Budai, R. Bock, A. Maier, J. Hornegger, and G. Michelson, “Robust vessel segmentation in fundus images,” International journal of biomedical imaging, vol. 2013, 2013.

[39] J. Sivaswamy, A. Chakravarty, G. Datt Joshi, T. Abbas Syed, JSM BIOMEDICAL IMAGING DATA PAPERS A Comprehensive Retinal Image Dataset for the Assessment of Glaucoma from the Optic Nerve Head Analysis, JSM Biomed Imaging Data Pap 2 (1) (2015) 1–7.

[40] S. Choi, “sjchoi86-HRF Database,” github.com/yiweichen04/retina_dataset, Accessed: 09-09-2019.

[41] P. Porwal, S. Pachade, R. Kamble, M. Kokare, G. Deshmukh, V. Sahasrabuddhe, and F. Meriaudeau, ‘‘Indian diabetic retinopathy image dataset (IDRiD): A database for diabetic retinopathy screening research,’’ Data, vol. 3, no. 3, p. 25, Jul. 2018

[42] Staal, J.J. Abramoff, M.D. Niemeijer, M. Viergever, and M.A. Ginneken, B. 2004. Ridge based vessel segmentation in color images of the retina. IEEE Transactions on Medical Imaging. 501-509. DOI= 10.1109/TMI.2004.825627

[43] Messidor-2 Data is Available for Researchers in the Public Domain At. Accessed: Jun. 18, 2019. [Online]. Available: https://medicine.uiowa.edu/eye/abramoff

[44] The new MIAS Database. http://www.wiau.man.ac.uk/services/MIAS/MIASfaq.html.

[45] M. Heath et al., "The digital database for screening mammography," in Proc. of the 5th Int. Workshop on Digital Mammography 431–434 (2000).

[46] Sung, J.; Ponce, C.; Selman, B.; Saxena, A. Unstructured human activity detection from rgbd images. In Proceedings of the 2012 IEEE International Conference on Robotics and Automation (ICRA), St. Paul, MN, USA, 14–18 May 2012; pp. 842–849

[47] Gasparrini, S.; Cippitelli, E.; Gambi, E.; Spinsante, S.; Wåhslén, J.; Orhan, I.; Lindh, T. Proposal and experimental evaluation of fall detection solution based on wearable and depth data fusion. In ICT Innovations 2015; Springer: Cham (ZG), Switzerland, 2016; pp. 99–108

[48] Junji Shiraishi, Shigehiko Katsuragawa, Junpei Ikezoe, Tsuneo Matsumoto, Takeshi Kobayashi, Ken-ichi Komatsu, Mitate Matsui, Hiroshi Fujita, Yoshie Kodera, and Kunio Doi. Development of a digital image database for chest radiographs with and without a lung nodule: receiver operating characteristic analysis of radiologists' detection of pulmonary nodules. American Journal of Roentgenology, 174(1):71–74, 2000

[49] Wang X, Peng Y, Lu L, Lu Z, Bagheri M, Summers RM. ChestX-Ray8: Hospital Scale Chest X-Ray Database and Benchmarks on Weakly-Supervised Classification and Localization of Common Thorax Diseases. In: 2017 IEEE Conference on Computer Vision and Pattern Recognition (CVPR), Honolulu, July 21–26, 2017. Piscataway, NJ: IEEE, 2017; 3462–3471.

[50] Summers RM. NIH Chest X-ray Dataset of 14 Common Thorax Disease Categories. https://nihcc.app.box.com/v/ChestXray-NIHCC/file/220660789610. Accessed May 2019.

[51] http://challenge2017.isic-archive.com/

[52] Amin, J., Sharif, M., Yasmin, M. and Fernandes, S.L., 2020. A distinctive approach in brain tumor detection and classification using MRI. *Pattern Recognition Letters*, *139*, pp.118-127.

[53] Saba, T., Mohamed, A.S., El-Affendi, M., Amin, J. and Sharif, M., 2020. Brain tumor detection using fusion of hand crafted and deep learning features. *Cognitive Systems Research*, *59*, pp.221-230.

[54] Rehman, A., Khan, M.A., Saba, T., Mehmood, Z., Tariq, U. and Ayesha, N., 2021. Microscopic brain tumor detection and classification using 3D CNN and feature selection architecture. *Microscopy Research and Technique*, *84*(1), pp.133-149.

[55] Yu, S., Xiao, D., Frost, S. and Kanagasingam, Y., 2019. Robust optic disc and cup segmentation with deep learning for glaucoma detection. *Computerized Medical Imaging and Graphics*, *74*, pp.61-71.

[56] Serte, S. and Serener, A., 2019, October. A generalized deep learning model for glaucoma detection. In *2019 3rd International symposium on multidisciplinary studies and innovative technologies (ISMSIT)* (pp. 1-5). IEEE.

[57] Bajwa, M.N., Singh, G.A.P., Neumeier, W., Malik, M.I., Dengel, A. and Ahmed, S., 2020, July. G1020: A Benchmark Retinal Fundus Image Dataset for Computer-Aided Glaucoma Detection. In *2020 International Joint Conference on Neural Networks (IJCNN)* (pp. 1-7). IEEE.

[58] Pour, A.M., Seyedarabi, H., Jahromi, S.H.A. and Javadzadeh, A., 2020. Automatic detection and monitoring of diabetic retinopathy using efficient convolutional neural networks and contrast limited adaptive histogram equalization. *IEEE Access*, *8*, pp.136668-136673.

[59] Kanjanasurat, I., Purahong, B., Pintavirooj, C., Satayarak, N. and Benjangkaprasert, C., 2020, September. Blood Vessel Extraction and Optic Disk Localization for Diabetic Retinopathy. In *Proceedings of the 2020 10th International Conference on Biomedical Engineering and Technology* (pp. 112-116).

[60] Arumugam, K., 2021. Chaotic Duck Traveler Optimization (cDTO) Algorithm for Feature Selection in Breast Cancer Dataset Problem. *Turkish Journal of Computer and Mathematics Education (TURCOMAT)*, *12*(4), pp.250-262.

[61] Agarwal, R., Diaz, O., Lladó, X., Yap, M.H. and Martí, R., 2019. Automatic mass detection in mammograms using deep convolutional neural networks. *Journal of Medical Imaging*, *6*(3), p.031409.

[62] Martínez-Villaseñor, L., Ponce, H., Brieva, J., Moya-Albor, E., Núñez-Martínez, J. and Peñafort-Asturiano, C., 2019. UP-fall detection dataset: A multimodal approach. *Sensors*, *19*(9), p.1988.

[63] Gaál, G., Maga, B. and Lukács, A., 2020. Attention u-net based adversarial architectures for chest x-ray lung segmentation. *arXiv preprint arXiv:2003.10304*.

[64] Majkowska, A., Mittal, S., Steiner, D.F., Reicher, J.J., McKinney, S.M., Duggan, G.E., Eswaran, K., Cameron Chen, P.H., Liu, Y., Kalidindi, S.R. and Ding, A., 2020. Chest radiograph interpretation with deep learning models: assessment with radiologist-adjudicated reference standards and population-adjusted evaluation. *Radiology*, *294*(2), pp.421-431.

[65] Codella, N.C., Gutman, D., Celebi, M.E., Helba, B., Marchetti, M.A., Dusza, S.W., Kalloo, A., Liopyris, K., Mishra, N., Kittler, H. and Halpern, A., 2018, April. Skin lesion analysis toward melanoma detection: A challenge at the 2017 international symposium on biomedical imaging (isbi), hosted by the international skin imaging collaboration (isic). In *2018 IEEE 15th international symposium on biomedical imaging (ISBI 2018)* (pp. 168-172). IEEE.